ISSN 0021-3640, JETP Letters, 2022, Vol. 116, No. 5, pp. 293–299. © Pleiades Publishing, Inc., 2022.
Russian Text © The Author(s), 2022, published in Pis'ma v Zhurnal Eksperimental'noi i Teoreticheskoi Fiziki, 2022, Vol. 116, No. 5, pp. 284–291.

PLASMA, HYDRO- AND GAS DYNAMICS

Runaway Electrons at the Formation of a Positive Ionization Wave in Nitrogen and Air

D. V. Beloplotov[a], *, V. F. Tarasenko[a, b], and D. A. Sorokin[a]

[a] *Institute of High Current Electronics, Siberian Branch, Russian Academy of Sciences, Tomsk, 634055 Russia*
[b] *National Research Tomsk State University, Tomsk, 634050 Russia*
**e-mail: rff.qep.bdim@gmail.com*

Received July 18, 2022; revised July 25, 2022; accepted August 2, 2022

The generation of runaway electrons (REs) at a subnanosecond breakdown of a "plane–needle" gap caused by the development of a positive ionization wave starting from a grounded needle electrode (anode) has been studied experimentally for the first time. Using a four-channel ICCD camera, a Hamamatsu streak camera, and an original method for measuring the displacement current generated by an appearing and propagating ionization wave, the generation of REs has been studied together with the dynamics ionization waves in air and nitrogen at pressures from 20 to 100 kPa. Current pulses of REs shorter than 100 ps have been observed in air at pressures of 60 kPa and below and in nitrogen in the entire pressure range. Double current pulses of REs have been observed in both gases at pressures below 50 kPa. It has been established that the generation of REs occurs after the arrival of the ionization wave at the planar cathode rather than at its start near the needle electrode, as could be expected. The energy of REs under these conditions is lower than the breakdown voltage by a factor of 4 or more. The data obtained indicate that REs are generated in the cathode layer.

DOI: 10.1134/S0021364022601580

INTRODUCTION

The generation of runaway electrons (REs) in nanosecond discharges at atmospheric pressure is currently an ordinary widely studied phenomenon [1–14], interesting in itself and for understanding of the mechanisms of preliminary ionization of a gas ahead of the ionization wave front. The generation of REs in discharges formed in a sharply inhomogeneous electric field is particularly well studied because this phenomenon under these conditions is easily reproducible and is of practical interest [15]. A discharge in a sharply inhomogeneous electric field usually has a diffuse form both in pure atomic and molecular gases and in their mixtures, and the generated plasma has a high electron temperature and a low temperature of heavy particles [3]. The discharge is formed in the diffuse form in any gases (even in SF_6 [16]) at low and high pressures owing to the ionizing action of REs generated in the pre-breakdown stage of the discharge in the region of a high electric field strength both near the needle electrode and at the front of the ionization wave. However, this is true only in the case of the development of anode-directed (negative) ionization waves. In the case of the development of cathode-directed (positive) ionization waves, electrons propagate toward the anode. It is suggested that X rays emitted by decelerating REs can ensure the preliminary ionization of the gas ahead of the front of positive ionization waves. However, the generation of REs under these conditions has never been studied by direct experimental methods. Only measurements of X rays were performed by different methods independently of the dynamics of the subnanosecond breakdown, and there are theoretical studies [3, 14, 16–20]. Any reliable published data on the possibility of generating REs under these conditions are absent. What mechanisms are responsible for the RE generation? Do electrons enter the runaway regime in a high electric field near the needle anode or at the front of the positive ionization wave? What is their energy? It is important to answer these question to understand the development of positive ionization waves in pure gases. Nevertheless, discharges in the sharply inhomogeneous electric field at the positive polarity have a diffuse form both in pure gases and in mixtures in a wide pressure range [3, 16]. Existing models describe well the formation of such discharges in air, where the preliminary ionization of the gas is ensured by the ionization of oxygen molecules by radiation from nitrogen molecules [21–27]. However, REs play a significant role even in the formation of negative ionization waves in air [28].

In this work, we attempt to detect current pulses of REs upon the development of positive ionization waves and to determine when and where REs are generated. To this end, we use a new method for studying a discharge by means of the measurement of the displacement current generated by the redistribution of

the electric field in the process of formation of the plasma [29, 30]. It is known that a time-dependent electric field induces the displacement current. Displacement currents in the gas discharge gap can be due both to the variation of the external field (e.g., at increasing and decreasing voltage) and to the redistribution of the electric field caused by charged particles from the ionization of the gas. An appearing streamer (ionization wave), whose head has a volume charge, causes the redistribution of the electric field in the gap. Correspondingly, a displacement current appears. Its magnitude depends on both the velocity and the dimensions of the ionization wave. This displacement current was specifically called the dynamic displacement current (DDC). Previous measurements of the DDC together with the current of REs show that REs can be generated even after the breakdown of the gap [31, 32].

EXPERIMENTAL SETUP AND METHODS OF MEASUREMENTS

Studies were performed at the setup shown in Fig. 1a. A gas discharge chamber was equipped with two 1-m-long transmission lines ($Z = 75\ \Omega$) with built-in capacitive voltage dividers. They allow the simultaneous measurements of the incident voltage wave and the voltage wave reflected from the gap. The voltage across the gap was reconstructed right during the experiment using oscilloscope mathematical utilities. The current of REs was measured using a collector made of a Radiolab 5D-FB PVC coaxial cable ($Z = 50\ \Omega$) with the central wire 1.8 mm in diameter. The end of the cable without the outer shell was placed in a metallic tube 6 mm in diameter, which was a part of a grounded electrode. A copper diaphragm 1.8 mm in diameter was sealed in the end of the tube. The distance between the diaphragm and the end of the central wire of the cable was approximately 1 mm. Thus, a signal was formed only by REs moving toward the wire of the cable (collector). The grounded truncated cone electrode (transmittance of 40%) was made of a 100-μm-thick grid. The larger and smaller bases of the truncated cone had diameters of 6 and 2 mm, respectively. The edge of the smaller base of the truncated cone ensured an increase in the electric field strength, as shown in Figs. 1b and 1c. The distributions of the potential and electric field strength were calculated in the two-dimensional axisymmetric geometry using the ELCUT 4.1 software. The high-voltage truncated cone electrode was made of one aluminum piece. The larger base of the cone directed to the grounded electrode had a diameter of 22 mm and a rounded edge. The distance between the electrodes was 5 mm.

In the experiments, we used nanosecond voltage pulse generators based on the FID technology [33]. A GIN-55-01 generator produced negative-polarity voltage pulses with an amplitude of −37 kV, a FWHM duration of 0.7 ns, and a rise time of 0.7 ns at a matched load, whereas a GIN-50-1 generator formed positive-polarity voltage pulses with an amplitude of 12 kV, a FWHM duration of 13 ns, and a rise time of 2.2 ns.

To study the generation of REs in correlation with the dynamics of the formation of the positive ionization wave, it is necessary to measure the current of REs and the displacement current both separately and together.

Measurement of only the displacement current I_{displ}. In this case, the incidence of REs on the collector should be prevented. This was ensured by placing a printer paper sheet with a thickness of about 100 μm ahead of the diaphragm of the collector. About 100 waveforms were recorded in the experiment.

Measurement of only the current of REs I_{REs}. In this case, the displacement current should be excluded. To this end, a small-cell metallic grid was placed in the diaphragm. About 100 waveforms were also recorded in this experiment.

Measurement of the current of REs together with the displacement current $I_{\mathrm{REs}} + I_{\mathrm{displ}}$. Selecting grids with different sizes of cells, we ensured the conditions under which the current of REs and the displacement current were of the same order of magnitude. About 100 waveforms were also recorded in this experiment.

In the entire set of data, we chose and compared waveforms with the same breakdown time delay.

The formation of the discharge was studied by optical methods with a HSFC-PRO four-channel ICCD camera and a Hamamatsu C10910-05 streak camera during the measurements of the current of REs and the displacement current. The minimum exposure time of the ICCD camera was 3 ns. However, the time delay between the channels could be varied in the range of 0.2–3 ns. The input slit of the streak camera was oriented along a line that was perpendicular to the surface of the high-voltage electrode and passed through the edge of the grounded electrode. The width of the slit was 0.02 mm, which ensured a time resolution of about 10 ps.

Signals from the capacitive voltage divider and collector were recorded by a Tektronix MSO64B oscilloscope (8 GHz, 20 GS/s).

The gas discharge chamber was evacuated with a forevacuum pump and then filled with air or nitrogen. The pressure was varied in the range of 20–100 kPa.

RESULTS AND DISCUSSION

When negative-polarity voltage pulses with an amplitude of −37 kV, a FWHM duration of 0.7 ns, and a rise time of 0.7 ns were applied across the gap filled with air or nitrogen, a diffuse discharge was observed in the entire studied range of pressures. Separate diffuse channels were observed at a pressure of 100 kPa, but they were joined with decreasing pressure.

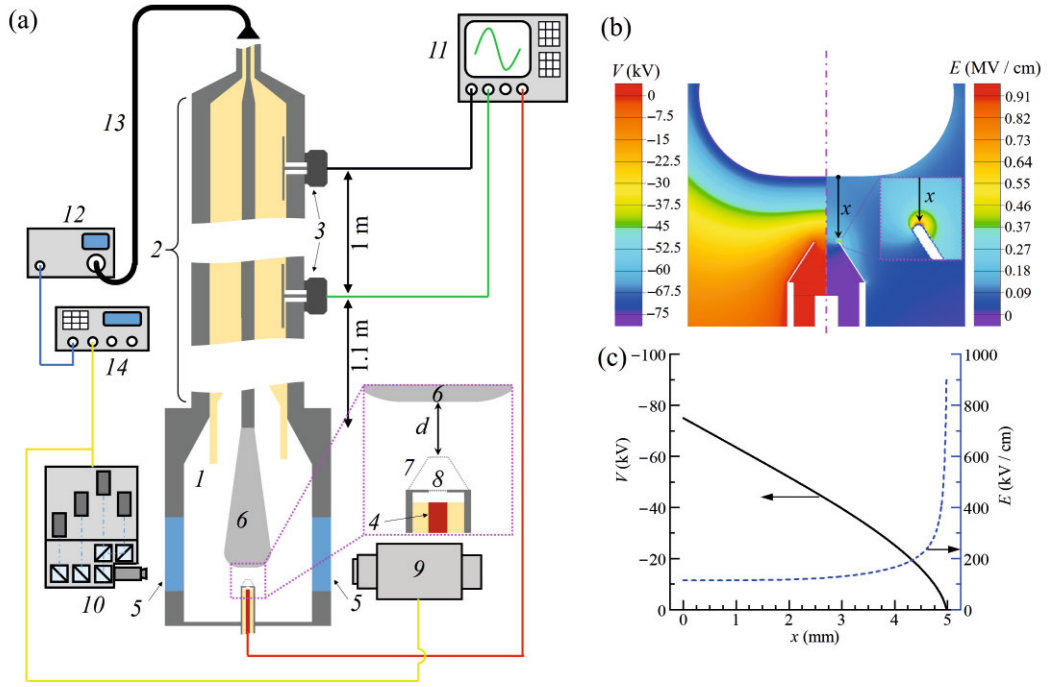

Fig. 1. (Color online) (a) Layout of the experimental setup: (*1*) gas discharge chamber, (*2*) coaxial transmission line, (*3*) capacitive voltage dividers, (*4*) receiving part of the collector (wire of the Radiolab 5D-FB PVC coaxial cable), (*5*) quartz window, (*6*) high-voltage electrode, (*7*) grounded grid electrode, (*8*) diaphragm with a grid or with a printer paper piece, (*9*) streak camera, (*10*) four-channel ICCD camera, (*11*) oscilloscope, (*12*) high-voltage generator, (*13*) high-voltage coaxial cable, and (*14*) triggering generator. (b, c) Distributions of the potential and electric field strength in the gas discharge gap.

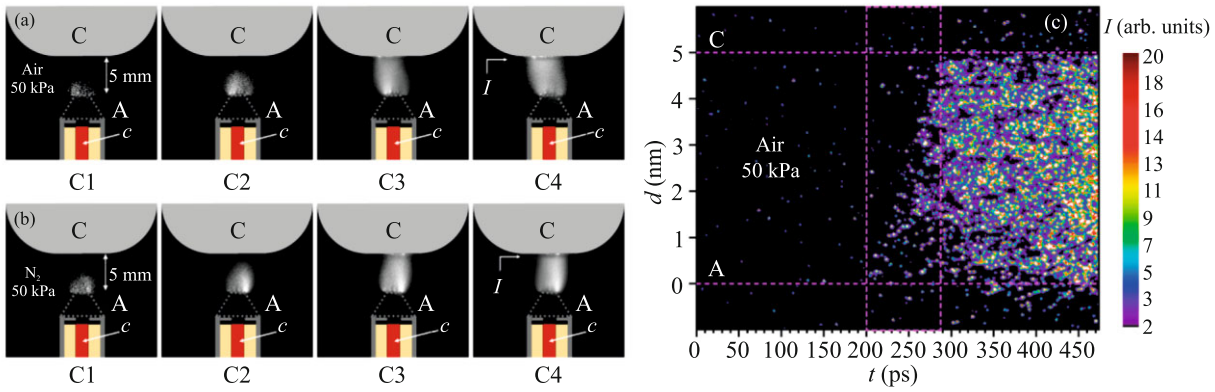

Fig. 2. (Color online) (a, b) Images of discharge plasma emission in air and nitrogen at a pressure of 50 kPa obtained by the four-channel ICCD camera: (C) cathode, (A) anode, (*c*) receiving part of the collector, and (*I*) dark space. (c) Time evolution of discharge plasma emission in air at a pressure of 50 kPa obtained with the streak camera.

Figures 2a and 2b show images of discharge plasma emission in (a) air and (b) nitrogen at a pressure of 50 kPa obtained by the four-channel ICCD camera at different times per one pulse. Images C1–C3 in Figs. 2a and 2b demonstrate the formation of the discharge and image C4 shows the total emission during the pulse. It is seen that the plasma appears near the grounded needle electrode (anode), where the electric field is enhanced (see Figs. 1a, 1b). The front of the plasma gradually propagates toward the planar high-voltage electrode; i.e., a positive ionization wave appears. After the bridging of the gap by the plasma, we observed the diffuse discharge, cathode and anode spots, and dark space near the cathode.

Time evolution of discharge plasma emission along the gap obtained with the streak camera in the first

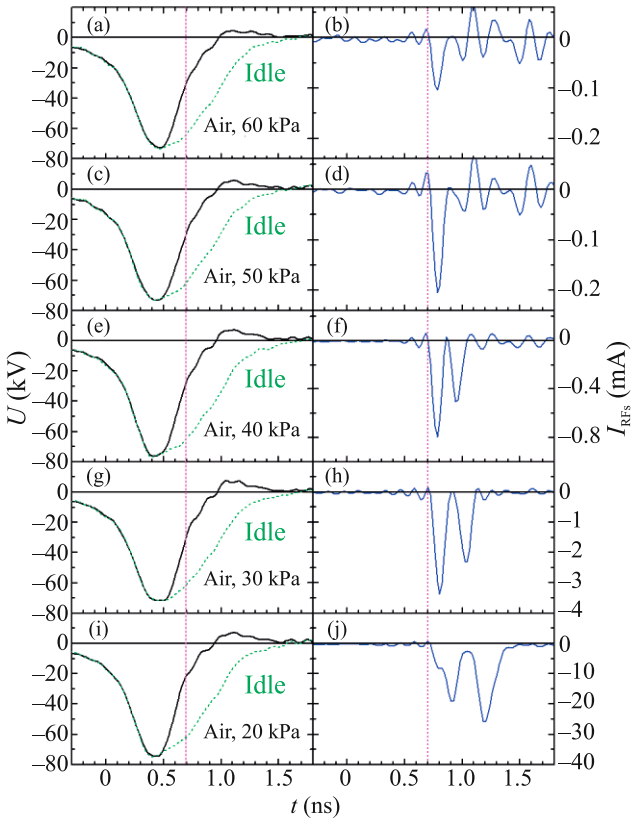

Fig. 3. (Color online) Waveforms of the voltage and current of runaway electrons recorded during the discharge in air at various pressures. The vertical dotted straight lines mark the time of detection of the current of runaway electrons on the collector with respect to the voltage across the gap.

several hundred picoseconds is shown in Fig. 2c. It also confirms that the formation of the plasma begins near the anode. It is seen that the front of the emission propagates from the anode to the cathode and bridges the gap in 80–90 ps. The average velocity of the positive ionization wave was ≈5.5 cm/ns. Under these conditions, we detected current pulses of REs.

Figure 3 presents the voltage and RE current waveforms during the discharge and idle modes in air. The idle mode was achieved after the evacuation of the gas discharge chamber by a forevacuum pump to a residual pressure of ~1 Pa. Under these conditions, the voltage pulse reflected from the gap was equivalent to the incident pulse.

The pressure of the gases was varied in the range of 20–100 kPa, but current pulses of REs in air were reliably detected at a pressure of 60 kPa and below. In the case of the discharge in nitrogen, REs were also observed at a pressure of 100 kPa. For demonstration, we chose pulses with close time delays of the breakdown differing by no more than 30 ps. It is also noteworthy that the length of the measuring line was not varied with the pressure. Only at a pressure of 20 kPa, an attenuator with a known delay was added in the measuring line.

It is seen that the amplitude of current pulses of REs increases with decreasing gas pressure, as expected. In the air pressure range of 30–60 kPa, the FWHM duration of pulses is 68 ps, which corresponds to the response time of the oscilloscope. This means that the real duration of current pulses of REs can be shorter. The duration of pulses at a pressure of 30 kPa and below exceeded 68 ps. A pair of current pulses of REs were observed at an air pressure of 40 kPa and below. The amplitude of the second pulse could exceed the amplitude of the first pulse.

The waveforms of current pulses of REs were matched to the voltage as described below. The position of current pulses of REs on the time scale with respect to voltage pulses that is marked by the dotted vertical straight line in Fig. 3 corresponds to REs reaching the collector.

The measurement of the displacement current induced by the ionization wave together with the current of REs by the collector allows one to determine the time of generation of REs with respect to the ionization wave [31, 32]. However, the displacement current was never measured previously in this configuration of the gas discharge gap, and it was first necessary to determine the amplitude–time parameters of the DDC generated by the ionization wave in the pure form without the effect of the displacement current induced by increasing or decreasing voltage and by the current of REs reaching the collector. A positive-polarity rectangular voltage pulse with a wide plateau and sufficiently fast rise and fall edges is ideal for these aims. The GIN-50-1 generator produces just such voltage pulses.

Figures 4a–4c present images of the discharge plasma emission in air at a pressure of 100 kPa recorded by the four-channel ICCD camera at the positive polarity per one pulse, as well as the corresponding voltage and the displacement current waveforms.

As in the case of negative polarity, the formation of the plasma begins near the grounded needle electrode, which serves as the cathode in this case. It is seen in Fig. 4a that several negative streamers move toward the high-voltage electrode (anode). However, only one of them finally forms a high-current channel (Fig. 4a, image C4). Figures 4b and 4c show the voltage and displacement current waveforms corresponding to this implementation of the discharge, as well as to the idle mode. The displacement current waveform (Fig. 4c) was matched to the voltage pulse through the capacitive current $I_C = CdU/dt$, where C is the capacitance of the gap and U is the voltage. It is seen that the appearance of the plasma near the grounded needle electrode (cathode) is accompanied by the generation of the displacement current because of the fast redis-

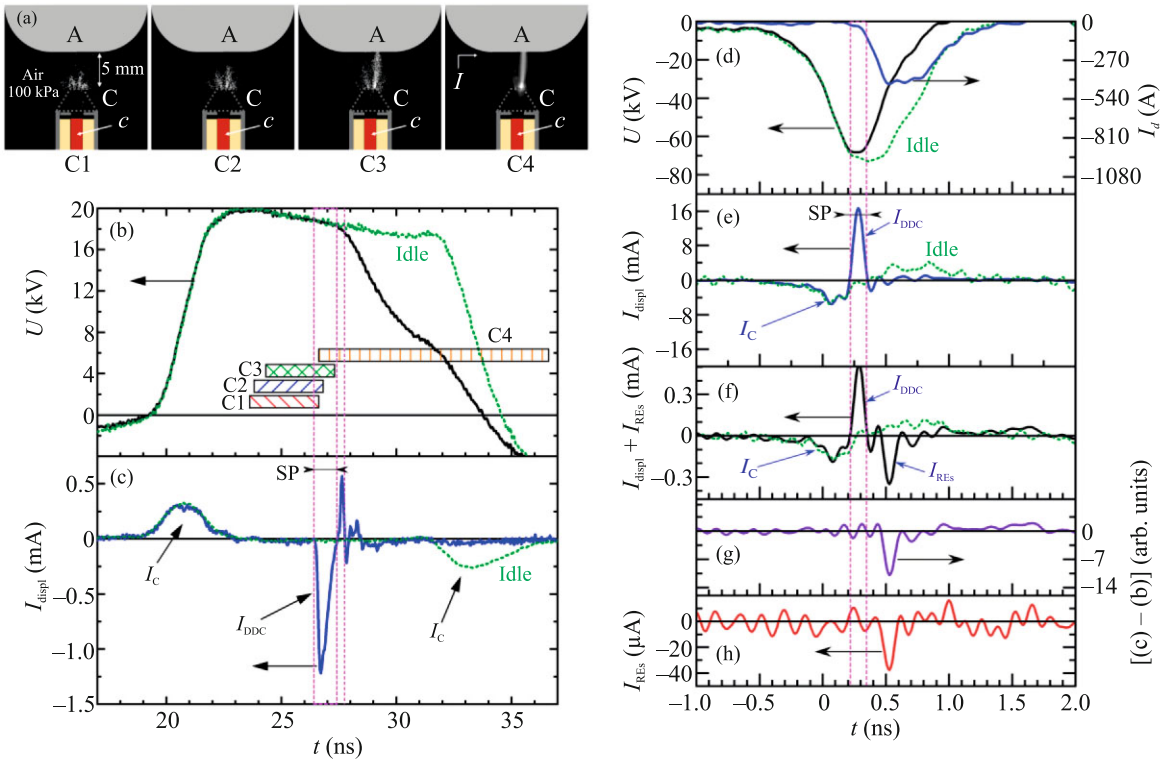

Fig. 4. (Color online) (a) Images of discharge plasma emission recorded by the four-channel ICCD camera at positive polarity: (A) anode, (C) cathode, (*c*) receiving part of the collector, and (C1–C4) channels of the ICCD camera. (b, c) Corresponding waveforms of the voltage and displacement current during the (solid lines) discharge and (dotted lines) idle modes, rectangles C1–C4 indicate the operating time intervals of the respective camera channels, and SP marks the streamer propagation stage. (d) Waveforms of voltage and discharge current during (solid lines) the discharge and (dotted lines) in the idle mode at negative polarity. (e) Waveforms of displacement current during (solid lines) the discharge and (dotted lines) in the idle mode at negative polarity. (f) Waveforms of (dotted lines) the displacement current in the idle mode and (solid lines) the sum of the current of runaway electrons and displacement current. (g) Difference between the signals in panels (f) and (e). (h) Waveform of the measured current of runaway electrons. Panels (a)–(c) and (d)–(h) refer to the discharge in air and nitrogen at a pressure of 100 kPa, respectively.

tribution of the electric field. This current is the DDC. The polarity of the DDC signal indicates that the electric field strength near the grounded needle electrode drops sharply when the plasma appears near it. When the DDC signal crosses the zero level, the electric field strength near the needle electrode reaches a local minimum. However, the backward ionization wave then reaches this region and the electric field strength begins to increase (positive polarity of the DDC). It is seen that the voltage across the gap decreases after that because the breakdown occurs. The average velocity of the streamer estimated from the duration of the negative-polarity DDC signal is ≈0.5 cm/ns.

Similar voltage and displacement current waveforms but at the negative polarity of the planar high-voltage electrode were obtained in nitrogen at a pressure of 100 kPa (see Figs. 4d–4h). In this case, the displacement current and the current of REs were measured simultaneously (see Fig. 4f). The current of REs and the displacement current had the same order of magnitude in the experiment with the 1-mm-cell grid made of wires 100 μm in diameter. Figures 4d and 4e show the (d) voltage and (e) displacement current waveforms during the (solid lines) discharge and (dotted lines) in the idle modes. The displacement current waveforms are matched to the voltage waveforms through the capacitive current $I_C = CdU/dt$. As in the case of positive polarity (Figs. 4a–4c), the appearance and propagation of the cathode-directed ionization wave are accompanied by the DDC. The DDC signal (Fig. 4e) exactly indicates when the streamer appears and bridges the gap. According to the duration of the DDC, the average velocity of the streamer was ≈4 cm/ns.

Figure 4f shows the sum of the displacement current and the current of REs measured simultaneously, and Fig. 4g presents the difference between the signals shown in Figs. 4f and 4e. The current waveform of REs measured without the DDC is presented in Fig. 4h for comparison. It is seen that the beam of REs (Fig. 4g) reaches the collector ≈250 ps later than the DDC signal induced by the streamer. If the electron beam were

generated near the grounded needle electrode (anode), whose edge was located at a distance of 4 mm from the collector, at the start of the positive ionization wave, so the energy of these electrons would be ~0.7×10^3 eV (i.e., $v \sim 1.6 \times 10^9$ cm/s), which is hardly possible. Another variant is the generation of REs in the cathode layer after the bridging the gap by the plasma. This mechanism of the generation of REs occurs after the breakdown of the needle–plane gap at voltages of 10–100 kV [31, 32], as mentioned in the Introduction. In this case, to estimate the energy of electrons, a distance of 9 mm from the cathode to the collector should be taken into account, and the time delay of the current pulse of REs should be measured from the time when the streamer reaches the cathode (≈110 ps). In this case, the energy of electrons is ~2×10^4 eV (i.e., $v \sim 8.3 \times 10^9$ cm/s). These estimates correlate with the energy of electrons measured by the foil method, where either a 10-μm-thick aluminum foil or 2-μm-thick dielectric kimfol film coated with aluminum 0.2 μm thick, which are transparent to electrons with energies of approximately 32 and 10 keV, respectively, was placed in front of the diaphragm of the collector. Thus, single RE beam current pulses in the studied gas pressure range were observed only with the kimfol film.

The results reported above indicate that REs are generated in the region of the cathode potential drop, where the electric field strength can exceed the critical strength necessary for electrons to enter the runaway regime and can ensure the emission of electrons from the cathode owing to field electron emission and the photoelectric effect and at the ion bombardment of the cathode surface. This hypothesis is also supported by a decrease in the amplitude of current pulses of REs by a factor of 2 or more when the planar high-voltage cathode was covered by 100-μm-thick Teflon film. If REs were generated near the grounded needle electrode (anode) or at the front of the positive ionization wave, the Teflon film did not affect the parameters of the current of REs.

CONCLUSIONS

To summarize, the reported experimental studies have shown that runaway electrons are generated during the breakdown of "plane–needle" gaps, which is due to the development of a positive ionization wave. However, the mechanism of their generation is fundamentally different from the case where the breakdown is caused by the development of a negative ionization wave. Runaway electrons are generated after the plasma bridges the gap rather than at the start of the ionization wave or at its front. After the positive ionization wave reaches the planar cathode, the volume positive charge at its front apparently leads to the formation of a cathode layer with a high electric field strength, which ensures the emission of electrons from the cathode. Some of these emitted electrons can enter the runaway regime. The result obtained in this work extends the representation of generation of runaway electrons in nanosecond discharges in a sharply inhomogeneous electric field. Together with previously obtained results, this indicates that the formation of the cathode layer and the generation of runaway electrons in it are ordinary phenomena accompanying nanosecond gas discharges. This effect can be both favorable and unfavorable because of the generation of accompanying X rays. This particularly concerns devices based on a discharge in helium for which the critical electric field strength is about one-fourth of that for nitrogen [2].

FUNDING

This work was supported by the Russian Foundation for Basic Research (project no. 20-02-00733) and by the Ministry of Science and Higher Education of the Russian Federation (state assignment no. FWRM-2021-0014 for the Institute of High Current Electronics, Siberian Branch, Russian Academy of Sciences).

CONFLICT OF INTEREST

The authors declare that they have no conflicts of interest.

REFERENCES

1. L. P. Babich, *High-Energy Phenomena in Electric Discharges in Dense Gases: Theory, Experiment, and Natural Phenomena* (Futurepast, Arlington, 2003).
2. Yu. D. Korolev and G. A. Mesyats, *Physics of Pulsed Breakdown in Gases* (Nauka, Moscow, 1991; Akad. Nauk, Yekaterinburg, 1993).
3. *Runaway Electrons Preionized Diffuse Discharges,* Ed. by V. F. Tarasenko (Nova Science, New York, 2014).
4. Y. Li, Y. Fu, Z. Liu, H. Li, P. Wang, H. Luo, X. Zou, and X. Wang, Plasma Sources Sci. Technol. **31**, 045027 (2022).
5. G. A. Mesyats, E. A. Osipenko, K. A. Sharypov, V. G. Shpak, S. A. Shunailov, M. I. Yalandin, and N. M. Zubarev, IEEE Electron Dev. Lett. **43**, 627 (2022).
6. E. I. Bochkov, L. P. Babich, and I. M. Kutsyk, Plasma Phys. Rep. **47**, 1027 (2021).
7. D. Levko, J. Appl. Phys. **126**, 083303 (2019).
8. V. V. Lisenkov, Y. I. Mamontov, and I. N. Tikhonov, J. Phys.: Conf. Ser. **2064**, 012021 (2021).
9. E. Oreshkin, Eur. Phys. Lett. **136**, 15001 (2021).
10. A. Kozyrev, V. Kozhevnikov, and N. Semeniuk, Plasma Sources Sci. Technol. **29**, 125023 (2020).
11. A. V. Kozyrev, E. M. Baranova, V. Yu. Kozhevnikov, and N. S. Semenyuk, Tech. Phys. Lett. **43**, 804 (2017).
12. V. Y. Kozhevnikov, A. V. Kozyrev, N. S. Semeniuk, and A. O. Kokovin, Russ. Phys. J. **61**, 603 (2018).
13. Y. Rybin, N. Kalinin, and M. Timshina, IEEE Trans. Plasma Sci. **49**, 1262 (2021).

14. A. Y. Starikovskiy, N. L. Aleksandrov, and M. N. Shneider, J. Appl. Phys. **129**, 063301 (2021).
15. K.-D. Weltmann, J. F. Kolb, M. Holub, D. Uhrlandt, M. Šimek, K. Ostrikov, S. Hamaguchi, U. Cvelbar, M. Černák, B. Locke, A. Fridman, P. Favia, and K. Becker, Plasma Process Polym. **16**, 1800118 (2018).
16. V. F. Tarasenko, D. V. Beloplotov, M. I. Lomaev, and D. A. Sorokin, J. Chem. Chem. Eng. **8**, 1156 (2014).
17. V. F. Tarasenko, E. Kh. Baksht, A. G. Burachenko, and M. I. Lomaev, Plasma Phys. Rep. **43**, 792 (2017).
18. J. R. Dwyer, Z. Saleh, H. K. Rassoul, D. Concha, M. Rahman, V. Cooray, J. Jerauld, M. A. Uman, and V. A. Rakov, J. Geophys. Res. Atmos. **113**, D23207 (2008).
19. C. V. Nguyen, A. P. J. van Deursen, E. J. M. van Heesch, G. J. J. Winands, and A. J. M. Pemen, J. Phys. D: Appl. Phys. **43**, 025202 (2010).
20. A. V. Kozyrev, V. Y. Kozhevnikov, I. D. Kostyrya, D. V. Rybka, V. F. Tarasenko, and D. V. Schitz, Atmos. Ocean Opt. **25**, 176 (2012).
21. M. B. Zheleznyak, A. K. Mnatsakanyan, and S. V. Sizykh, High Temp. **20**, 357 (1982).
22. A. A. Kulikovsky, J. Phys. D: Appl. Phys. **33**, 1514 (2000).
23. S. Pancheshnyi, Plasma Sources Sci. Technol. **24**, 015023 (2015).
24. N. Y. Babaeva, D. V. Tereshonok, and G. V. Naidis, Plasma Sources Sci. Technol. **25**, 044008 (2016).
25. J. Teunissen and U. Ebert, Plasma Sources Sci. Technol. **25**, 044005 (2016).
26. A. Bourdon, F. Péchereau, F. Tholin, and Z. Bonaventura, Plasma Sources Sci. Technol. **30**, 105022 (2021).
27. A. Brisset, K. Gazeli, L. Magne, S. Pasquiers, P. Jeanney, E. Marode, and P. Tardiveau, Plasma Sources Sci. Technol. **28**, 055016 (2019).
28. N. Y. Babaeva, G. V. Naidis, D. V. Tereshonok, and E. E. Son, J. Phys. D: Appl. Phys. **51**, 434002 (2018).
29. D. V. Beloplotov, M. I. Lomaev, V. F. Tarasenko, and D. A. Sorokin, JETP Lett. **107**, 606 (2018).
30. D. V. Beloplotov, M. I. Lomaev, D. A. Sorokin, and V. F. Tarasenko, Phys. Plasmas **25**, 083511 (2018).
31. D. V. Beloplotov, V. F. Tarasenko, V. A. Shklyaev, and D. A. Sorokin, JETP Lett. **113**, 129 (2021).
32. D. V. Beloplotov, V. F. Tarasenko, V. A. Shklyaev, and D. A. Sorokin, J. Phys. D: Appl. Phys. **54**, 304001 (2021).
33. V. M. Efanov, M. V. Efanov, A. V. Komashko, A. V. Kirilenko, P. M. Yarin, and S. V. Zazoulin, in *Ultra-Wideband, Short Pulse Electromagnetics 9,* Ed. by F. Sabath, D. V. Giri, F. Rachidi-Haeri, and A. Kaelin (Springer, New York, 2010), Part 5, p. 301.

Translated by R. Tyapaev